NACA

RESEARCH MEMORANDUM

DAMPING IN ROLL OF A MISSILE CONFIGURATION WITH

A MODIFIED TRIANGULAR WING AND A CRUCIFORM

TAIL AT A MACH NUMBER OF 1.52
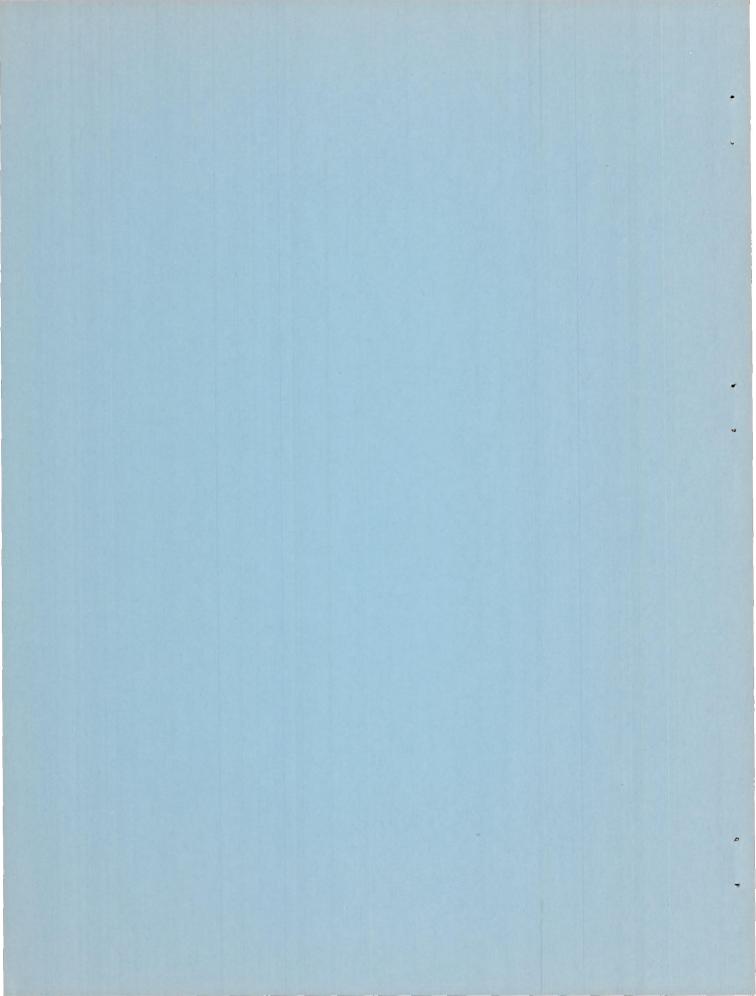
By Richard Scherrer and David H. Dennis

Ames Aeronautical Laboratory
Moffett Field, Calif.

NATIONAL ADVISORY COMMITTEE
FOR AERONAUTICS
WASHINGTON
March 6, 1951

NATIONAL ADVISORY COMMITTEE FOR AERONAUTICS

RESEARCH MEMORANDUM

DAMPING IN ROLL OF A MISSILE CONFIGURATION WITH

A MODIFIED TRIANGULAR WING AND A CRUCIFORM

TAIL AT A MACH NUMBER OF 1.52

By Richard Scherrer and David H. Dennis

SUMMARY

The damping-in-roll stability derivatives of a missile configuration and its components were determined both experimentally and theoretically. The tests were conducted at a Mach number of 1.52 and at a Reynolds number, based on the mean aerodynamic chord of the wing, of 0.82×10^6.

The experimental damping derivative of the wing-body combination was 67 percent of the theoretical value. The difference is believed to have resulted mainly from the fact that the theory is not strictly applicable when the Mach number normal to the leading edge is almost unity, which was the case in the present investigation. For the tail-body combination the damping derivative was 86 percent of the theoretical value. In this case, the difference is believed to have been caused partially by mutual interference between the tail surfaces and partially by the low Reynolds number of the flow over the tail. It was found that the damping of the complete configuration was not equal to the sum of the damping derivatives of the components because of the effect of the wing downwash on the damping of the tail.

INTRODUCTION

The resistance to roll, or the damping in roll, is a major factor in determining the dynamic lateral stability of an aircraft and therefore must be predictable with good accuracy. Values of the damping-in-roll stability derivative for isolated wings have been calculated by the use of linearized theory for a variety of wing plan forms (references 1, 2, and 3), and experimental investigations have been conducted with wings of triangular and rectangular plan forms (references 4, 5, and 6). The

effect of a body on the theoretical damping–in–roll coefficient of an isolated wing has been treated in references 7 and 8. It was found that, for both subsonic and supersonic wing leading edges, the presence of a body, the diameter of which is less than one–third of the wing span, has a small (less than 4 percent) effect on the damping coefficient of the wing.

The prediction of the damping of a complete configuration having a wing and a tail, however, is complicated by the influence of the wing on the flow over the tail, and thus the damping derivatives of components cannot be added directly to obtain the damping of the complete configuration. The present investigation was undertaken to measure the damping–in–roll characteristics of a missile configuration and its components and to compare the results with linearized theory.

The experimental investigation was made at the request of the U. S. Air Force, and the model, the strain–gage balance, and the model–spinning apparatus were supplied by the Boeing Airplane Company. The wing–body combination of the present investigation was identical to that used in the lateral–control and dihedral–effect tests reported in reference 9.

NOTATION

b wing span, 4.74 inches

C $\tan \epsilon$

C_l rolling–moment coefficient $\left(\dfrac{L}{qSb}\right)$, dimensionless

C_{l_p} damping–in–roll stability derivative $\left[\dfrac{\partial C_l}{\partial(pb/2V)}\right]$, dimensionless

c local wing chord, inches

$\overline{c}$ wing mean aerodynamic chord, 1.86 inches

$$\left(\overline{c} = \frac{\displaystyle\int_0^{b/2} c^2 \, dy_b}{\displaystyle\int_0^{b/2} c \, dy_b}\right)$$

d distance from wing trailing edge to tail leading edge at the tail mean aerodynamic chord

$E'(\beta C)$ complete elliptic integral of the second kind with modulus $\sqrt{1-\beta^2 C^2}$

$F'(\beta C)$ complete elliptic integral of the first kind with modulus
$\sqrt{1-\beta^2 C^2}$

L rolling moment about body axis, inch-pounds
(Positive moments are clockwise when the aircraft is viewed from the rear.)

M Mach number, dimensionless

P local lifting pressure on wing, pounds per square inch

p angular velocity of roll, radians per second

q free-stream dynamic pressure, pounds per square inch

r radius from y_1 to y'

Re Reynolds number based on wing mean aerodynamic chord, dimensionless

S total wing area (including that within the body), 8.78 square inches

V free-stream velocity, inches per second

w downwash velocity perpendicular to radius r at the tail surface, inches per second

w' downwash velocity perpendicular to tail surface, inches per second

x,y,z coordinates relative to wing vortex sheet with origin at wing apex

X_L streamwise distance from wing apex to any point on wing leading edge

X_T streamwise distance from wing apex to any point on wing trailing edge

y_b spanwise coordinate in wing-chord plane with origin at wing apex

y_1 variable point of integration in y direction at tail

y',z' coordinate system at the tail where y' and z' are the spanwise axes of the cruciform tail

β $\qquad$ $\sqrt{M^2-1}$

Γ $\qquad$ local circulation on wing, inches squared per second

ϵ $\qquad$ half of wing apex angle, radians

μ $\qquad$ Mach angle $\left(\mu = \sin^{-1}\frac{1}{M}\right)$, degrees

ρ $\qquad$ air density in free stream, slugs per cubic inch

APPARATUS

The experiments were performed in the Ames 1- by 3-foot supersonic wind tunnel No. 1. This closed-circuit variable-density wind tunnel is equipped with a nozzle having flexible top and bottom plates which can be shaped to give test section Mach numbers between 1.2 and 2.4. The absolute total pressure in the wind tunnel can be varied from 1/5 of an atmosphere to about 3 atmospheres depending on the Mach number and the ambient air temperature. The air in the wind tunnel is dried to an absolute humidity of 0.0001 pound of water per pound of dry air in order to make the effects of condensation in the nozzle negligible.

The model used in the tests consisted of a body of revolution that had an ogival nose and a fineness ratio of 16 in combination with a modified triangular plan-form wing and a cruciform tail. The important dimensions of the model are given in figure 1. For the present tests the wing and ailerons were set parallel to the body center line. The 0.01-inch-wide gaps at the wing-body and wing-aileron junctures were unsealed because it was assumed that their effects would be small at zero incidence and zero aileron angle. The wing leading-edge sweepback angle was slightly greater than the complement of the Mach angle at the test Mach number, 1.52, but the tail sweepback angle was less than this angle, as shown in figure 1. The wing, which was demountable, and two after bodies, one with tail surfaces and one without, were used in three combinations (body plus wing, body plus tail, and body plus wing plus tail) to obtain the desired data. The model was attached to a sting-type support, and the sting was mounted in ball bearings so that the model and sting were free to rotate about their longitudinal axis. Rotation of the model was produced by a two-bladed windmill shown in figure 2. The angle of the blades could be adjusted to obtain different rotational speeds. The rolling moment, or the damping in roll, was measured by electrical-resistance strain gages mounted within the sting near the forward end. The electrical connections to the strain gages passed through slip rings which were located at the rear of the bearing housing. (See fig. 2.)

TESTS

The damping moment of each of the three model configurations was measured at several rolling velocities to determine the damping—in—roll stability derivative C_{l_p}. All the tests of the present investigation were conducted at a Mach number of 1.52 at an absolute total pressure of 18 pounds per square inch. The Reynolds number of these tests, based on the mean aerodynamic chord of the wing, was 0.82 million.

The strain—gage balance was calibrated statically in the wind tunnel just prior to the tests and zero—load readings were made before and after each test as a continuous check on the instrumentation. The rotational speed of the model was measured by calibrated stroboscopic light and the rolling moments and rotational speeds were measured simultaneously. The tests were conducted at rotational speeds ranging from 2000 to 4000 rpm. In addition, the body—wing—tail combination was tested at zero rotational speed to determine the static rolling moment due to model asymmetry and variations in the wind—tunnel air stream.

The body of the model was so long that the conical bow wave, when reflected from the wind—tunnel side walls, passed between the wing and the tail. It is believed that this reflected shock wave had a negligible effect on the damping derivatives because the wave was initially weak and its effect was further reduced by being reflected from the flat walls of the wind tunnel. Although some small asymmetries existed in the model and the air stream, the damping derivatives are not affected because even though the vertical positions of the curves (C_l vs $pb/2V$) are altered by such irregularities the slopes remain unchanged. Estimates of the errors in measurement in each of the variables entering into the presentation of the data are given in the following table:

Variable	Estimated error
C_l	±1.5 percent
p	± 20 rpm
$pb/2V$	±1 percent
M	±0.01
C_{l_p}	± 2 percent
Re	± 20,000

RESULTS AND DISCUSSION

The experimental values of rolling-moment coefficient for the three
configurations are shown as functions of wing-tip helix angle in figure 3.
The three lines in figure 3 do not pass through the origin, indicating
that some asymmetries existed in the models and the air stream. The
results and the comparisons with linearized theory will be discussed
separately for each configuration.

Wing-Body Combination

Theoretical results shown in references 7 and 8 indicate that the
damping derivative for wing-body combinations should not vary with rate of
roll $pb/2V$ for a given model at a given Mach number and indicate that
the body of this test should have a negligible effect on the damping of
the wing. The data for the wing-body combination, which is presented in
figure 3, appear to lie along a line of constant slope, and it is believed
that the damping derivative of the combination is constant within the
test range of wing-tip helix angles.

The theoretical damping-in-roll derivative of the wing alone was
calculated by the method given in reference 1 assuming the raked-in tips
to be located along Mach lines. The theoretical and experimental values
are noted in table I and show the value of the experimental damping deriv-
ative to be 67 percent of the theoretical value. The difference is
believed to be due to the fact that the wing leading edge and the Mach
cone from the wing apex were almost coincident at the test Mach number
(consequently the velocity component normal to the leading edge was in
the transonic regime). Linearized theory does not include the effects of
the transonic flow near the wing leading edge and therefore cannot be
expected to give accurate results at these test conditons. The rather
low Reynolds number of the tests (0.82×10^6) also may have contributed
to the difference between theory and experiment.

The effect on the damping derivative of the proximity of the wing-
apex shock wave to the leading edge is shown by the data for triangular
wings presented in reference 4. In these tests, the experimental values
of the derivatives were about 10 percent less than the theoretical values
when the wing-apex shock wave and the leading edge were far from coinci-
dent, but when they were almost coincident the difference between the
theoretical and experimental values increased from 20 to 25 percent. The
Reynolds numbers of these tests at the Mach number (1.62) at which the
leading edge and the apex bow wave were nearly coincident were almost the
same as the Reynolds number in the present tests. If the differences in
the models in the two investigations are considered, the results appear
to be in agreement.

Because of the complexity in calculating the exact damping—in—roll stability derivative of triangular wings with cut—off tips, several short—cut methods were considered. The most obvious simplification when the change in wing area due to the wing—tip modification is small is to ignore the change from the original triangular wing and use its damping deriv—ative in stability calculations. The theoretical damping derivative of the wing alone was calculated for actual plan form and the triangular plan form, and the results are shown below:

1. Considering effect of the raked—in wing tips, $C_{l_p} = -0.287$

2. Ignoring effect of wing—tip modification, $C_{l_p} = -0.280$

The change in wing area due to the modification amounted to 6 percent of the wing area, and it is apparent from the foregoing comparison that the corresponding change in the damping—in—roll stability derivative is small. It should be remembered, however, that in the calculation of the rolling moment (L) and the rolling—moment coefficient (C_l) from the stability derivative (C_{l_p}) the actual wing span and area must be used.

Tail—Body Combination

Data for the tail—body combination could only be obtained in a nar—row range of rotational speeds because the model vibrated severely out—side this range. A straight line was drawn through the data points (fig. 3) and it was found that the sum of the ordinates at zero rate of roll for the wing—body and tail—body combinations is almost equal to the corresponding ordinate for the complete configuration. This fact tends to substantiate the belief that the experimental value of the damping derivative is constant.

Although the change in tail area due to cutting off the tips in a streamwise direction was small (approximately 4 percent of the tail area), the modification results in a loss of lift in the tip region of the remaining portion of the tail. As a result of this additional loss in lift, the assumption that the damping derivative was that of a triangular wing does not seem likely to be as satisfactory for the tail as it was for the wing. The theoretical damping derivative of the tail was calcu—lated by using the data for triangular wings given in reference 2 but with the following corrections for the effect of streamwise tips. The pressure distribution in the vicinity of the tip of the full triangular wing was computed and the amount of damping due to the load on the cut—off tip was determined. The effect of the streamwise tip on the pressure distribution on the tail within the Mach cone from the tip leading edge was approxi—mated by arbitrarily assuming the spanwise lift distribution to fall

linearly from the value at the Mach cone to zero at the tip. The damping
moments of these two regions were subtracted from the damping moment of
the complete triangular plan form and a new damping derivative was calcu-
lated based on the actual tail span and area. This derivative, for four
tail fins, was based on the total tail area and amounted to −0.316
while the damping derivative of the corresponding triangular surfaces was
−0.291. The agreement between these values is not as good as for the
wing perhaps because the good agreement obtained with the wing was fortu-
itous.

The theoretical damping-in-roll derivative of the tail alone, when
based on the wing span and area, is −0.132. As shown in table I, the
experimental value is 86 percent of the theoretical value for the wing-
tail combination. Part of the difference between theory and experiment
is believed to be mutual interference between the tail surfaces. A theo-
retical investigation of this effect for wings swept well within the Mach
cone is reported in reference 10. This theory indicates that for slender
wings the interference reduces the damping derivative by 19 percent. In
the present experiments, however, the leading edges of the tail surfaces
were swept ahead of the Mach cone from the apex. As a result, the inter-
ference effect should be much less than that for a highly swept cruciform
wing because the fraction of the wing area over which the interference
can occur is less.

The results of tests of a single wing, with a triangular plan form
and with the same location of the wing leading edge relative to the apex
Mach cone as that in this test, are reported in reference 4. The tests
were conducted at a Reynolds number similar to that of the present tests,
0.51×10^6 based on the tail mean aerodynamic chord, and the results
indicate a difference between theory and experiment of 10 percent.

Wing-Tail-Body Configuration

The sum of the experimental damping derivatives for the body-wing
and body-tail combinations, as noted in table I, is −0.303 while the
damping derivative of the body-wing-tail combination is −0.240. The dif-
ference between these two values is primarily due to the effect of the
downwash field of the wing on the flow over the tail surfaces. The sum
of the theoretical damping derivatives of the components (−0.414) is 70
percent greater than the experimental value for the complete configuration
(−0.240) because of the addition of the differences between theory and
experiment for the components to the wing-tail interference effect.

In an attempt to account for the effect of the wing downwash on the
damping derivative of the tail, a method of calculating the velocity field

at the tail has been derived and is given in detail in the appendix. The method consists of computing the downwash normal to the tail surfaces by using the theoretical, nondimensional, span load distribution on the wing and by assuming that the trailing vortex sheet from the wing remains plane at the tail. The coordinate system (in a plane normal to the body axis at the tail) that is used in the analysis is shown in figure 4.

If the theoretical, span load distribution is adjusted to correspond with the experimental damping of the wing, the downwash field at the tail can be computed with good accuracy within the limits imposed by the assumption of a plane vortex sheet. This assumption is apparently not as gross as might be expected, at least for the case of four tail surfaces, because it was found that the average downwash perpendicular to the tail surfaces at any spanwise position varied by only 10 to 15 percent through the range of possible positions of the vortex sheet relative to the tail planes. For this reason, it is expected that the average downwash over the tail would be changed only slightly by the rolling up of the vortex sheet that actually occurs.

The distribution of the downwash existing at the two tail planes, based on the theoretical damping derivative of the wing, is shown in figure 5 along with the local velocity due to roll. The average effective velocity distribution (difference between curves I and III in fig. 5) was obtained by assuming the theoretical curve to be continuous through the origin rather than discontinuous. This assumption with a wing mounted in a body is believed to be more reasonable than the theoretical curve for the wing alone.

Since the effective velocity distribution is nonlinear, the problem of determining the exact change in damping of the tail is extremely complex. For this reason, it was assumed that the effective velocity distribution could be linearized to give a velocity distribution such that the area beneath the linear distribution curve (curve V in fig. 5) and the area beneath the curve for the more exact distribution (curve IV in fig. 5) would be equal. With this assumption, the correction to the damping of the tail becomes, as shown in figure 5, the ratio of the ordinates of curves I and V.

It is possible that the accuracy of the method could be improved by use of a secondary correction based on the differences between curves IV and V in figure 5. Such a correction would probably be based on the product of the local tail chord, the spanwise moment arm, and the local difference between curves IV and V. However, the effects of the local tail chord and the spanwise moment arm are opposite and almost equal, therefore such a correction would be small for the present configuration and has been neglected.

Although it is very approximate the primary correction, when based on the experimental damping derivative of the wing, accounts for 63 percent of the effect of the wing downwash on the damping in roll of the tail. As shown in table I, the sum of the damping derivatives of the body—wing combination and the corrected experimental damping derivative of the body—tail combination is only 10 percent greater than the measured value for the complete configuration.

CONCLUSIONS

The results of an investigation of the damping—in—roll characteristics of a missile configuration and its components and a theoretical investigation of the influence of the wing downwash on the damping of the tail in steady roll lead to the following conclusions:

1. The damping—in—roll derivative for the wing—body combination tested was found to be only 67 percent of the theoretical value, probably because of the proximity of the wing apex Mach line to the wing leading edge.

2. The experimental damping—in—roll derivative of the tail—body combination was 86 percent of the theoretical value. The difference is believed to have been caused partially by mutual interference between the tail surfaces and partially by the low Reynolds number of the flow over the tail.

Ames Aeronautical Laboratory,
    National Advisory Committee for Aeronautics,
        Moffett Field, Calif.

APPENDIX

CALCULATION OF THE EFFECT OF WING DOWNWASH ON THE

VELOCITY FIELD AT THE TAIL OF AN AIRCRAFT

IN STEADY ROLL

In order to predict the damping in roll of an aircraft, the damping characteristics of the wing alone and tail alone must be known. The change in velocity distribution normal to the tail surfaces resulting from the presence of the wing can be calculated from the load distribution on the wing, and the change in velocity can be used to obtain a correction to the tail—alone damping in roll. This method is dependent upon the following major assumptions in addition to those normally made in linearized wing theory:

1. The helical trailing vortex sheet from the wing remains straight in all transverse cross sections (does not roll up at the edges) and its longitudinal axis is not displaced from the longitudinal axis of the wing.

2. The spanwise downwash distribution at the tail can be linearized ($w'=ky'$) so as to obtain an effective rate of roll.

A diagram of the coordinate system (in a plane normal to the body axis at the tail) that is used in the following analysis is shown in figure 4. The induced velocity w at any point y,z is the summation over the span of the vortex sheet of the velocities induced by the elemental trailing vortices, or, in differential form

$$dw = \frac{d\Gamma/dy_1}{2\pi r} \, dy_1 \qquad (1)$$

The induced velocity w' normal to the tail chord plane at any spanwise station on the tail y' when the cosine of the angle ζ (fig. 4) is evaluated becomes

$$w' = w \cos\zeta = \frac{1}{2\pi y'} \int_{-b/2}^{b/2} \frac{d\Gamma}{dy_1} \left(\frac{y'^2 - yy_1}{y'^2 - 2yy_1 + y_1^2} \right) \, dy_1 \qquad (2)$$

It should be noted that

$$y' = y/\cos\lambda \qquad (3)$$

where the angle λ is the angular displacement of the tail relative to the vortex sheet from the wing and its value is given by the equation

$$\lambda = 45° \pm \frac{180}{\pi} \frac{pd}{V} \tag{4}$$

where d is the distance from the wing trailing edge to the leading edge of the mean aerodynamic chord of the tail.

The rate of change of circulation with spanwise position $d\Gamma/dy_1$ can be obtained from the following equation based on the span load distribution of the wing:

$$\frac{d\Gamma}{dy_1} = \frac{d}{dy_1}\left[\frac{V}{2} \int_{x_L}^{x_T} \left(\frac{\Delta P}{q} \right) dx \right] \tag{5}$$

where $\Delta P/q$ is the local lifting pressure coefficient at a point x,y on the wing with the origin of the coordinate system at the wing apex. This coefficient for a rolling triangular wing with subsonic leading edges is given in reference 3 by the following equation:

$$\frac{\Delta P}{q} = \frac{4xpC^2\theta}{V\left[\frac{2-\beta^2 C^2}{1-\beta^2 C^2} E'(\beta C) - \frac{\beta^2 C^2}{1-\beta^2 C^2} F'(\beta C) \right]\sqrt{C^2-\theta^2}} \tag{6}$$

where θ is equal to y_1/x

For a triangular wing at the test Mach number and with the same leading-edge sweepback as the wing of the present investigation, equation (6) becomes:

$$\frac{\Delta P}{q} = 1.246 \frac{p}{V} \frac{xy_1}{\sqrt{0.729x^2-y_1^2}} \tag{7}$$

Substitution of equations (3), (5), and (7) in equation (2) gives the relation:

$$w' = \frac{1.246p}{4\pi y'} \int_{-b/2}^{b/2} \left(\frac{d}{dy_1} \int_{x_L}^{x_T} \frac{xy_1}{\sqrt{0.729x^2-y_1^2}} dx \right) \left(\frac{y'^2-y_1y'\cos\lambda}{y'^2-2y_1y'\cos\lambda+y_1^2} \right) dy_1$$

$$\tag{8}$$

Since the damping derivative of the wing plan form used on the model has been shown to be almost equal to that of an equivalent triangular wing, it is reasonable to use the geometry of the triangular wing to obtain the downwash distribution normal to tail planes. With this aproximation, equation (8) becomes

$$w' = 0.1982 \frac{p}{y'} \int_{-b/2}^{b/2} \left[(3.53 - 0.471y_1^2)^{1/2} - \frac{0.942y_1^2}{(3.53 - 0.471y_1^2)^{1/2}} \right] \times$$

$$\left(\frac{y'^2 - y'y_1\cos\lambda}{y'^2 - 2y'y_1\cos\lambda + y_1^2} \right) dy_1 \tag{9}$$

The downwash field at the tail is obviously a function of the angle λ and therefore the downwash effect for one of the tail planes, as can be seen from equation (4), varies with the rate of roll p. For cruciform tails, however, the average downwash effect is almost independent of the rate of roll because the changes in downwash at each tail plane are compensating. This compensation should increase for tails with more than four fins, but should decrease with a decrease in the number of tail fins. It should be noted that the rolling up of the vortex sheet that actually occurs quite rapidly with low-aspect-ratio wings will affect the downwash distribution at the tail. However, the effect of the rolling-up of the vortex sheet on the damping of the tail should decrease with an increasing number of fins.

REFERENCES

1. Margolis, Kenneth: Theoretical Lift and Damping in Roll of Thin
     Swept Back Tapered Wings with Rake—in and Cross—Stream Wing Tips
     at Supersonic Speeds; Subsonic Leading Edges. NACA TN 2048, 1950.

2. Jones, Arthur L., and Alksne, Alberta: The Damping Due to Roll of
     Triangular, Trapezoidal, and Related Plan Forms in Supersonic
     Flow. NACA TN 1548, 1948.

3. Brown, Clinton E., and Adams, Mac C.: Damping in Pitch and Roll of
     Triangular Wings at Supersonic Speeds. NACA Rep. 892, 1948.

4. Brown, Clinton E., and Heinke, Harry S., Jr.: Preliminary Wind—
     Tunnel Tests of Triangular and Rectangular Wings in Steady Roll
     at Mach Numbers of 1.62 and 1.92. NACA RM L8L30, 1949.

5. Sandahl, Carl A.: Free—Flight Investigation of the Rolling Effec—
     tiveness of Several Delta Wing—Aileron Configurations at Tran—
     sonic and Supersonic Speeds. NACA RM L8D16, 1948.

6. Martz, C. William, and Church, James D.: Flight Investigation at
     Subsonic, Transonic, and Supersonic Velocities of the Hinge—
     Moment Characteristics, Lateral—Control Effectiveness, and Wing
     Damping in Roll of a 60° Swept Back Delta Wing with Half—Delta
     Tip Ailerons. NACA RM L9L14, 1950.

7. Tucker, Warren A. and Piland, Robert O.: Estimation of the Damping
     in Roll of Supersonic—Leading—Edge Wing—Body Combinations.
     NACA TN 2151, 1950.

8. Lomax, Harvard, and Heaslet, Max. A.: Damping—in—Roll Calculations
     for Slender Swept—Back Wings and Slender Wing—Body Combinations.
     NACA TN 1950, 1949.

9. Scherrer, Richard, and Dennis, David H.: Lateral—Control Character—
     istics and Dihedral Effect of a Wing—Body Combination with a
     Variable—Incidence Triangular Wing and Wing—Tip Ailerons at a
     Mach Number of 1.52. NACA RM A50H10, 1950.

10. Adams, Gaynor J.: Theoretical Damping in Roll and Rolling Effec—
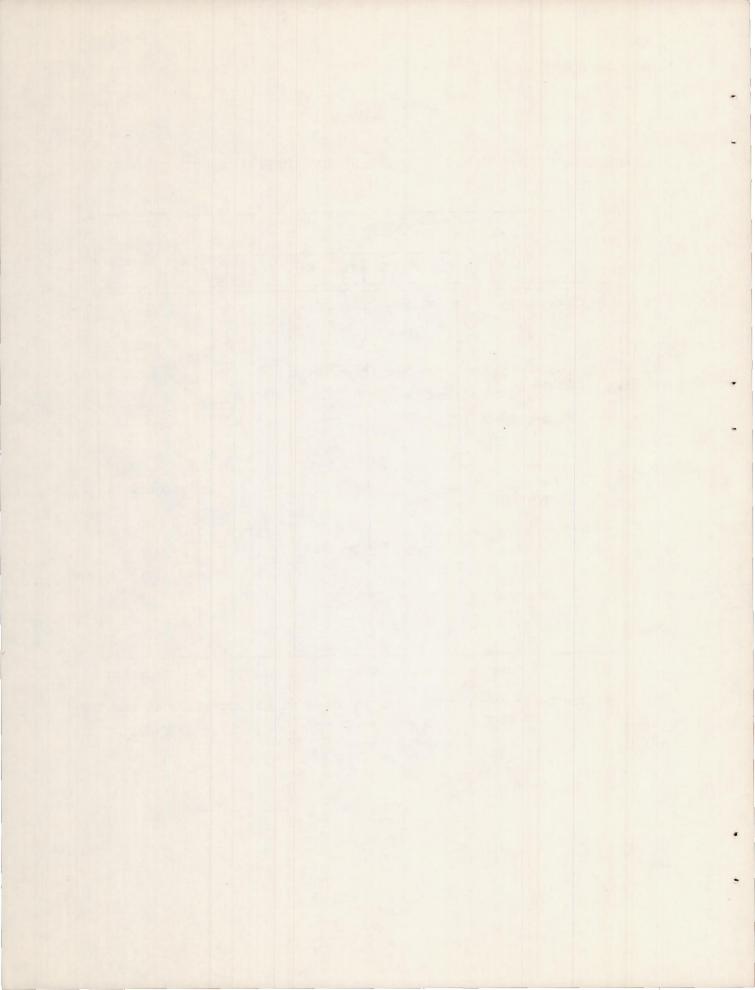   tiveness of Slender Cruciform Wings. NACA TN 2270, 1950.

TABLE I

COMPARISON OF THEORETICAL AND EXPERIMENTAL DAMPING-IN-ROLL DERIVATIVES

Configuration	C_{l_p}		$\dfrac{C_{l_{p_{exp}}}}{C_{l_{p_{theory}}}}$	References for theory
	Experiment	Theory		
(1) Body–wing	−0.194	−0.287	67 %	1 and 7
(2) Body–tail	−.109	−.127	86 %	2 and 7
(3) (Body–wing) + (Body–tail)	−.303	−.414	− −	− − − −
(4) Wing–body–tail	−.240	− −	− −	− − − −
(5) (Body–tail) Corrected for wing downwash	−.069*	−.053	− −	2, 7, and appendix A
(6) (Body–wing) + (Body–tail) Corrected for wing downwash (Line 1 + line 5)	−.263*	−.340	− −	− − − −

Note: All damping derivatives are based on wing span and area.

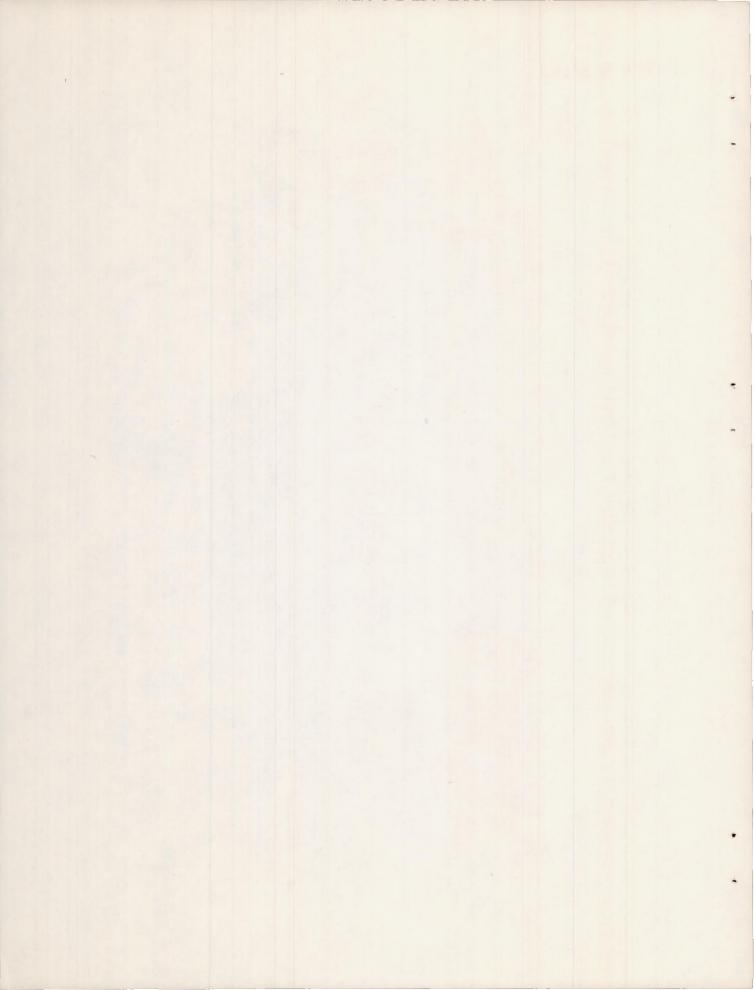* The theoretical correction is based on the experimental damping of the wing.

All dimensions in inches

Mach line

Front View

0.131 0.087

1.00

15.98

7.84

0.010

49½°

0.010

2.00

4.73

2.70

1.95

Strain gage balance

Plan View

Wing Wedge Angles
Normal to leading edge — 14½°
Normal to trailing edge — 10°

Tail Wedge Angles
Normal to leading edge — 11°
Normal to trailing edge — 8°

Mach line

1.34

0.34

1.70

0.050

39½°

0.50

Tail Plan Form
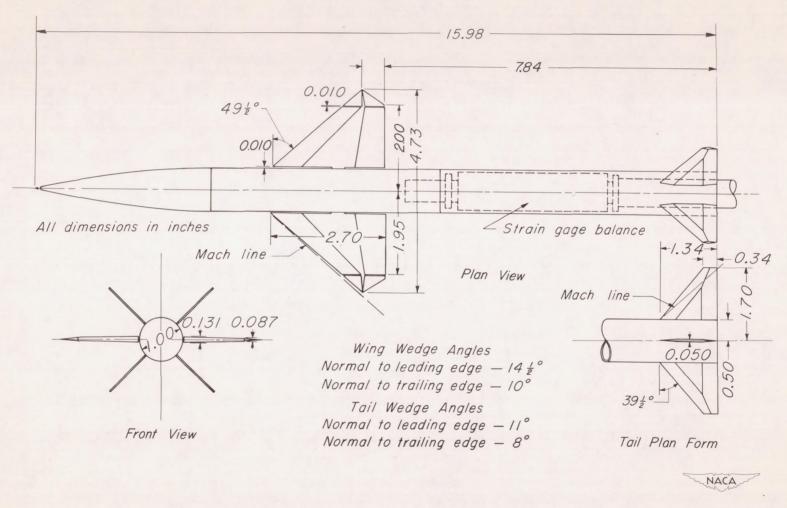
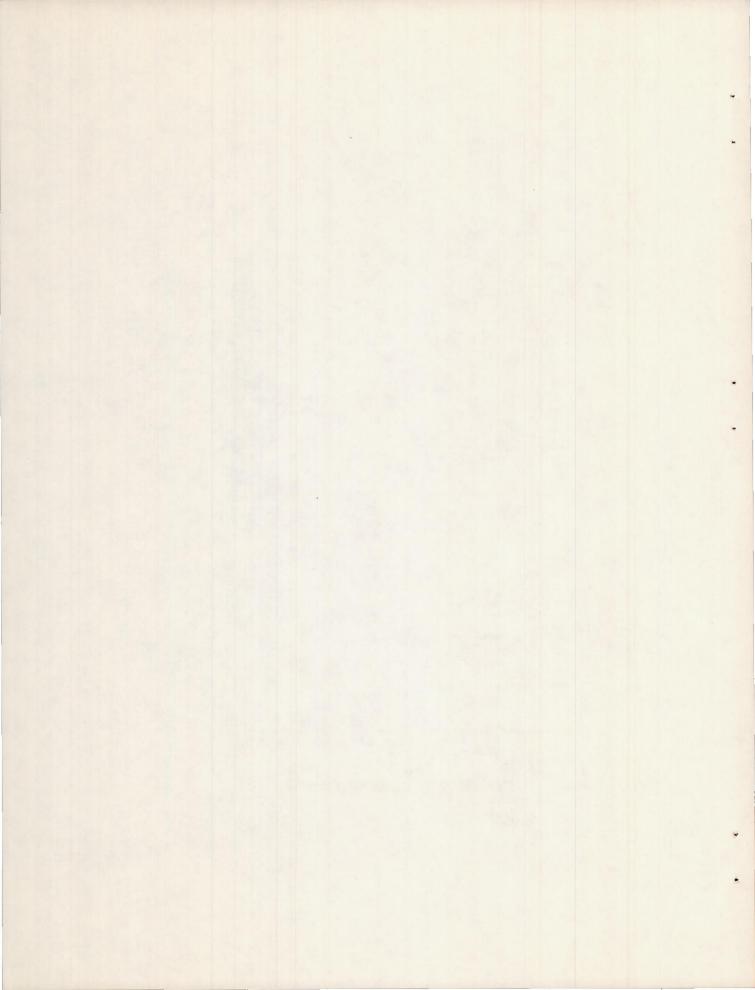Figure 1.— Dimensions & Details of Complete Model Configuration.
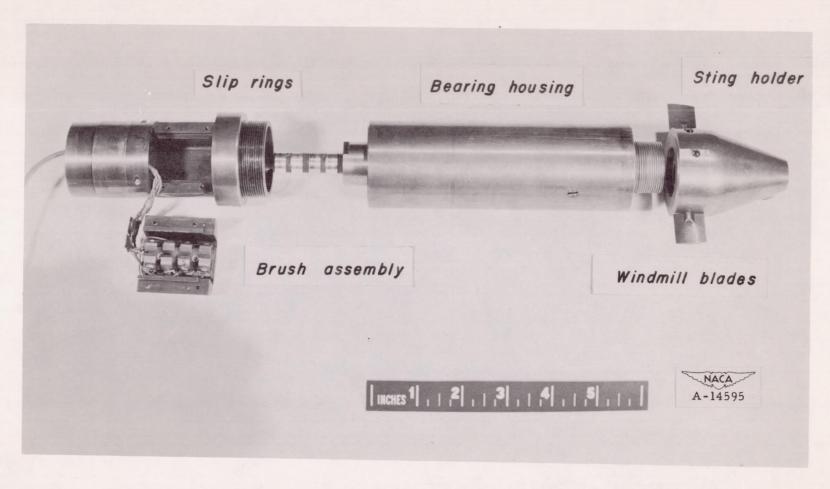
Figure 2.— Sting-and-model support housing.
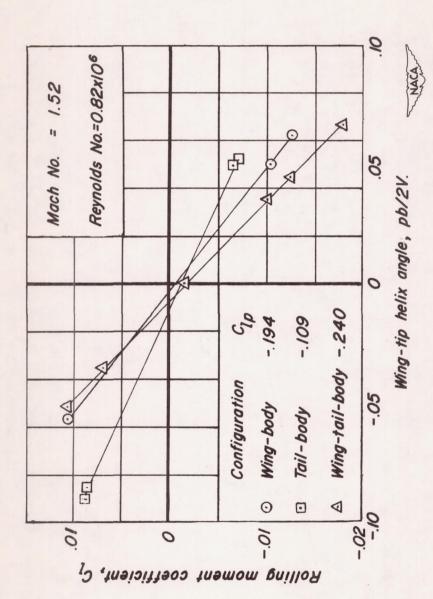
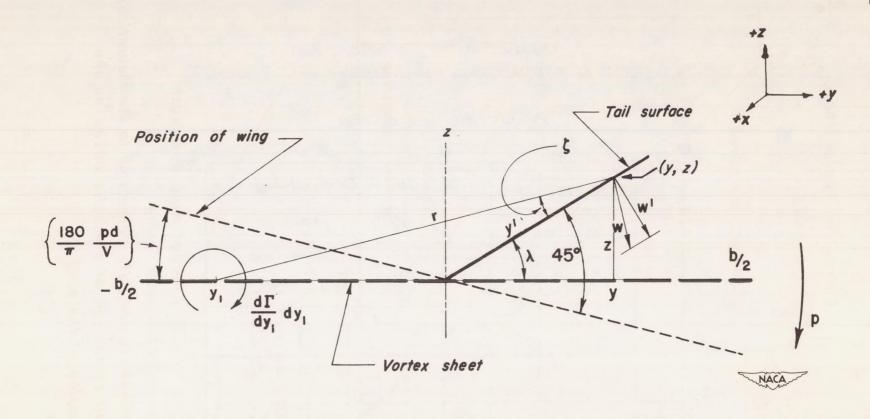Figure 3.- The damping-in-roll characteristics of a missile configuration and its components.

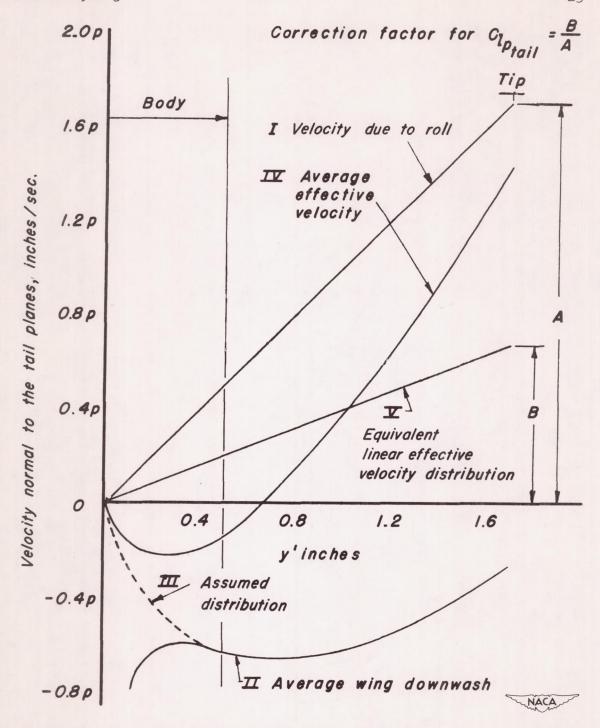Figure 4.- Coordinate system for calculation of the effect of the wing downwash on the damping in roll of the tail.

Figure 5.– Wing downwash–velocity correction to the theoretical damping in roll of the tail of a missile based on the theoretical damping of the wing.